Array Signal Processing

Daniel Levi

February 2024

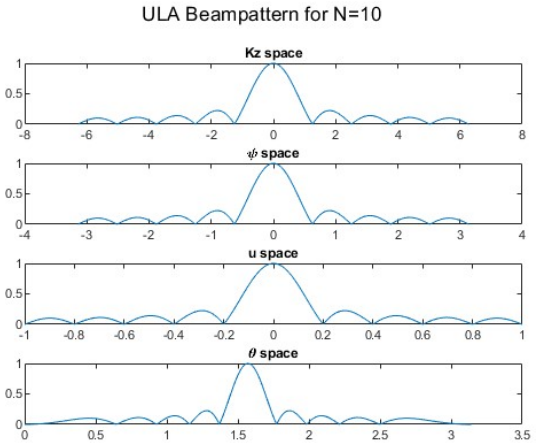

Figure 1: ULA beampattern for even number of sensors

Exercise 1: Beampattern of ULA

a)

Plot the magnitude of the beampattern in the k_z, Ψ, u, and Θ space.

given the connection $\psi = -k_z \cdot d = 2\pi/\lambda \cdot d \cdot cos(\Theta) = 2\pi/\lambda \cdot u_z \cdot d$ we can plot the beampattern as a function of k_z, Ψ, u and Θ.

Where:

$$k_z \in [-2\pi, 2\pi], \Psi \in [-\pi, \pi], u \in [-1, 1], \Theta \in [0, \pi]$$

in Figs. 1, 2 We observe the beam pattern. As seen in the classes, in this particular case, the beam pattern can be written as:

$$B(w_0, \Psi) = \frac{1}{N} \frac{sin(\frac{N\Psi}{2})}{sin(\frac{\Psi}{2})}$$

The number of zeros in this function depends on N, which explains the variation among different N values. Additionally, the main Dirichlet width also depends on N. If we plot both of them in the same figure 3 the difference will be more significant.

b)

Perform a polar plot of the powerpattern in the Θ-space for N = 10 and N = 11. Which significant difference can be observed?

The significant difference is in the number of beams. As can we see in figs. 4 , 5 the number of zeros depends on N and as long as N is bigger we will observed more zeros.

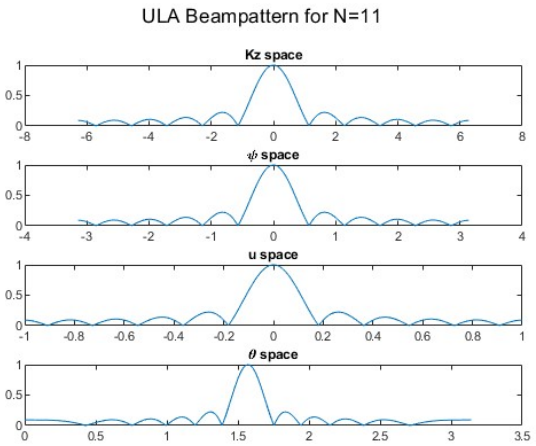

Figure 2: ULA beampattern for an odd number of sensors

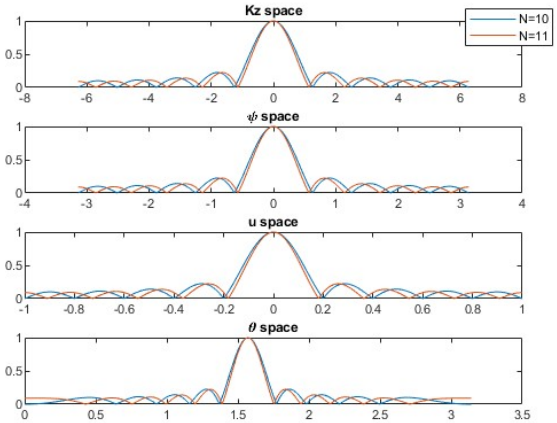

Figure 3: ULA beampattern

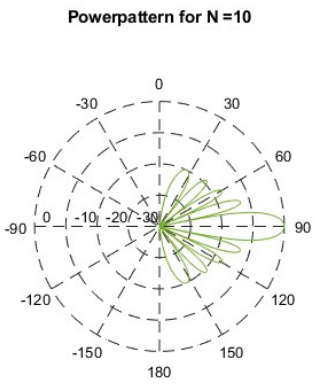

Figure 4: ULA powerpattern for even number of sensors

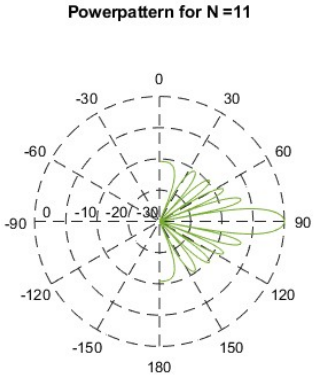

Figure 5: ULA powerpattern for an odd number of sensors

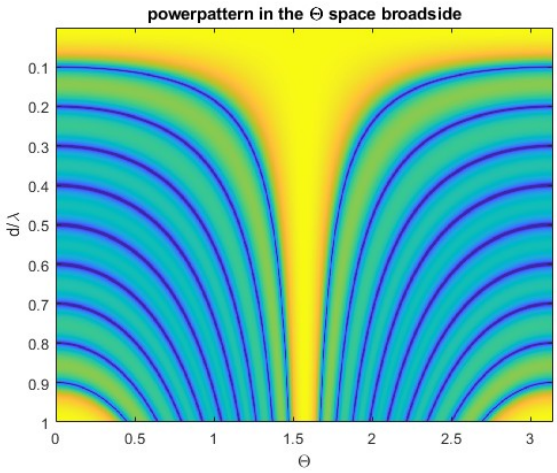

Figure 6: Broadside

c)

Plot the powerpattern in the Θ-space for $0.001 \leq d/\lambda \leq 1$. Compare the plots for broadside and endfire orientation w.r.t. mainlobe width and grating lobes. In fig. 6 we can see the powerpattern for the broadside. We can see that for small d/λ the main lob is wider and for large values for d/λ we can see the aliasing phenomena.

In fig. 7 we can see the powerpattern for the endfire. We can see that for small d/λ the main lob is wider and for $d/\lambda \geq 1/2$ there is a spatial aliasing in that case.

d)

Perform the previous plots in the Θ-domain for steering angles $\Theta_T \in \{0°, 30°, 60°, 90°\}$. What is the effect of the array steering on the main beam?

We can see from fig. 8 that for small angles the main beam is wider like endfire and when we increase the angle the beam becomes narrow(for a meaning chose d/λ).

e)

Due to sensor failure, $w_n = 0$ for $n \in \{3, 5, 6\}$. Plot the powerpattern for the array in the Ψ-domain with and without sensor failure in a single figure.

In fig. 9 we can see that the failure distorts the powerpattern. from the eq. that we see in class that:

$$B_\psi(\psi) = e^{-j\frac{N-1}{2}\psi} \sum_{n=0}^{N-1} w_n^* e^{jn\psi} = \frac{1}{11}\left(e^{-j5\psi} + e^{-j4\psi} + e^{-j3\psi} + e^{-j\psi} + e^{j2\psi} + e^{j3\psi} + e^{j4\psi} + e^{j5\psi}\right)$$

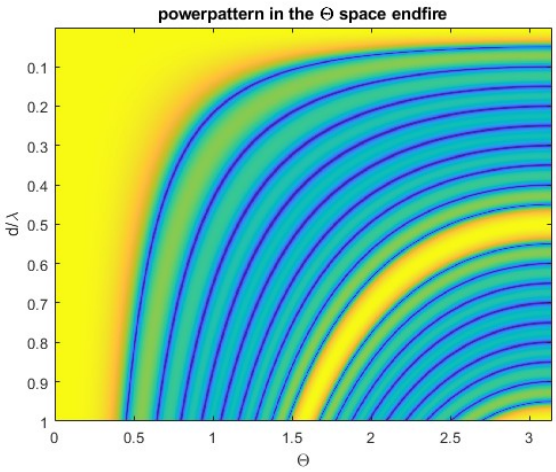

Figure 7: Endfire

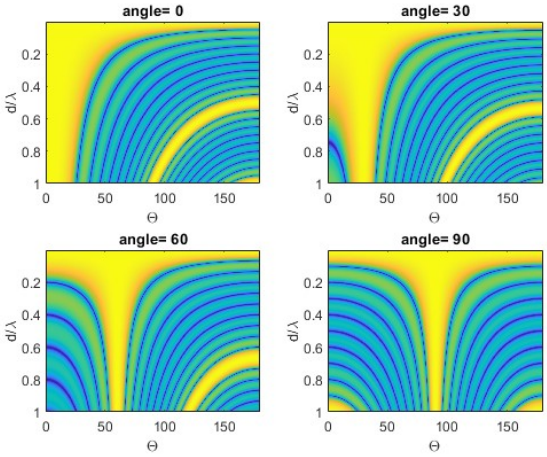

Figure 8: steering angles

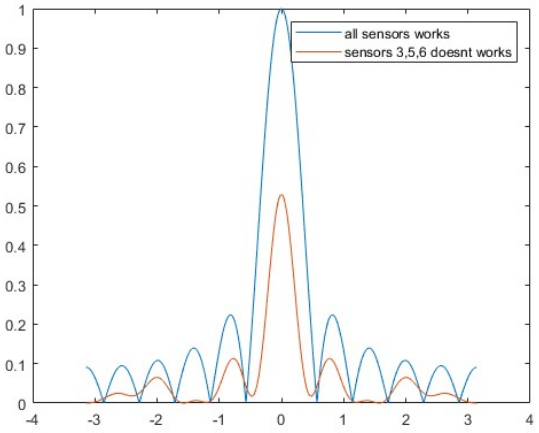

Figure 9: sensor failure

we can see that for $N = 11$:

$$B_{\psi}^{2}(0) = \left(\frac{8}{11}\right)^{2} \simeq 0.52$$

Moreover, the number of Nulls decreases and they move a bit.

Exercise 2: Non-uniform Weighting

An ULA with $N = 11$ sensors and $d = \lambda/2$ is considered. Two different weights are applied

$$w_I[n] = \frac{1}{N}$$

$$w_{II}[n] = sin(\frac{\pi}{2N})cos(\frac{\pi n}{N})$$

with $n = -\frac{N+1}{2}, -\frac{N-1}{2}, \ldots, \frac{N-1}{2}$.

Plot the u domain powerpatterns in dB in a single figure for both weights ($0 \leq u \leq 1$). What is the effect of the non-uniform weighting?

In fig. 10, we can observe the power patterns for uniform weights and non-uniform weights. The primary distinction is that in non-uniform weighting, the magnitude of side lobes is lower, and the main lobe is wider.

Exercise 3: Half-Power Bandwidth

Extend the script provided for this case:

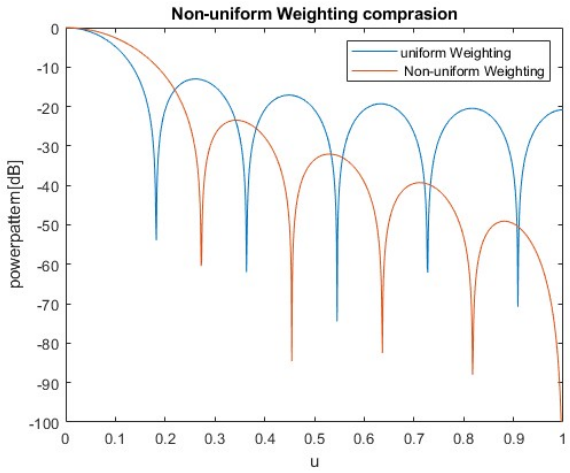

Figure 10: Non-uniform Weighting comprasion

a)

half-power beamwidth for the scan limit $\Theta_h^{(l)}$

In Fig. 11, we observe the beamwidth for the scan limit and endfire cases. In both scenarios, when Nd/λ is small, the beamwidth is high. This is logical because, in such instances, the beampattern is close to 1. In the scan limit case where $\Theta_l = 0$, we notice that the slope decreases gradually. Similarly, in the endfire case, the slope decreases slowly, consistent with what we discussed in class: $\Theta_h \approx 2\sqrt{0.886\lambda/Nd}$ because $\Theta_h = 2\Theta_r$.

b)

half-power beamwidth for the steering angles $\Theta_t \in \{2.5^\circ, 5^\circ, 10^\circ, 20^\circ, 30^\circ, 45^\circ, 90^\circ\}$

In Fig. 12 the slope is given by

$$\Theta_h \approx \frac{20.886}{sin(\Theta_t)} \frac{\lambda}{Nd}$$

and it behaves linearly (in logarithmic scale).

Exercise 4: Beampattern of MVDR Beamformer

An MVDR beamformer with $N = 10$ sensors, $d = \frac{\lambda}{2}$, and broadside orientation in the presence of a single discrete interference source and isotropic noise is considered. The weights of this MVDR beamformer are given by

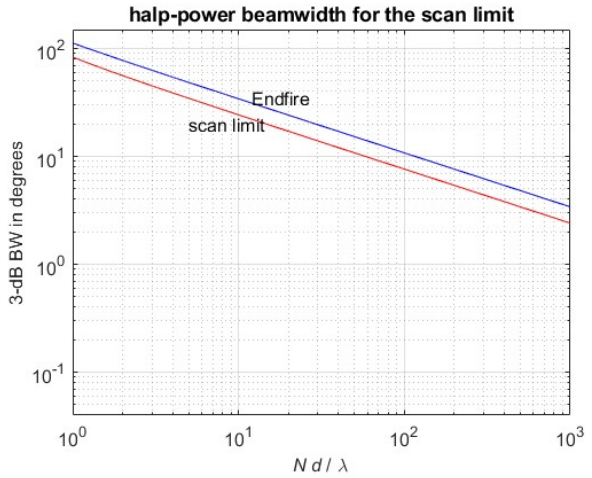

Figure 11: halp-power beamwidth for the scan limit

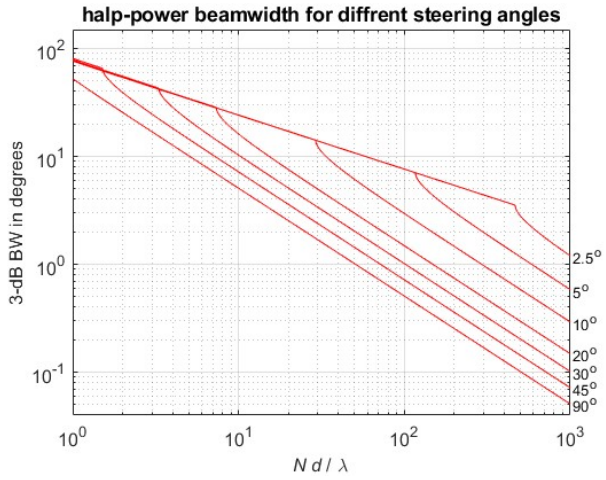

Figure 12: halp-power beamwidth for diffrent steering angles

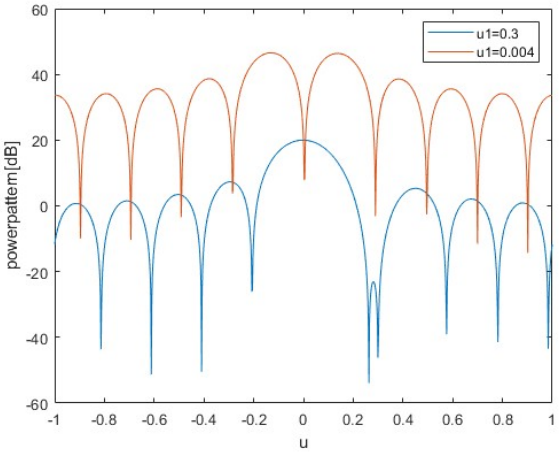

Figure 13: The power pattern of the MVDR beamformer

$$\mathbf{w}_O^H = \frac{\mathbf{v}_s^H \mathbf{S}_n^{-1}}{\mathbf{v}_s^H \mathbf{S}_n^{-1} \mathbf{v}_s} \tag{1}$$

with

$$\mathbf{S}_n = \sigma_w^2 \mathbf{I} + \sigma_1^2 \mathbf{v}_1 \mathbf{v}_1^H \tag{2}$$

The interference-to-noise ratio is given by

$$\sigma_I^2 = \frac{\sigma_1^2}{\sigma_w^2} \tag{3}$$

a)

Plot the power pattern in the u-domain for an interferer at $u_1 = 0.3$ and $u_1 = 0.004$ for an interference-to-noise ratio (INR) of 70 dB.

In Fig. 13, we can see the power pattern for two interference positions. In the orange curve, the interference position is at $u_1 = 0.004$, causing a null in the main lobe (the target at $u_t = 0$). Consequently, the power pattern remains at 0 dB. Conversely, in the case where the interference is positioned at $u_1 = 0.3$, there is a strong null (-20 dB).

b)

Perform a 3-dimensional plot of the power pattern for varying interferer directions with $0.001 \leq u_1 \leq 0.5$ and an interference-to-noise ratio (INR) of 70 dB. Redo this plot for an INR of 0 dB.

How does the direction of the interferer and the interference-to-noise ratio influence the powerpattern?

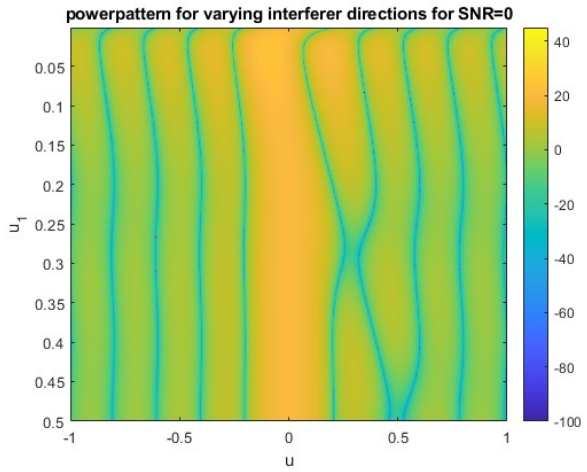

Figure 14: powerpattern for varying interferer directions for $INR = 0$dB

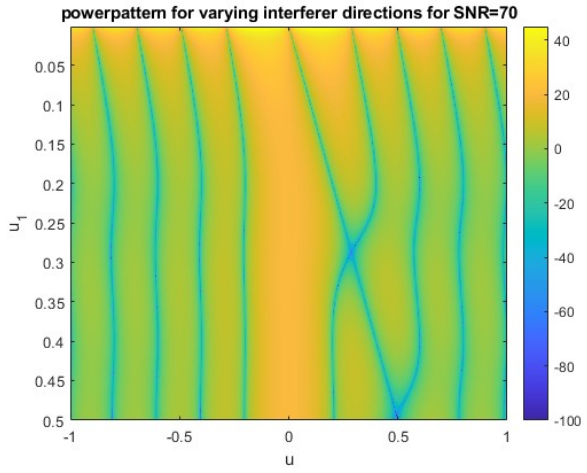

Figure 15: powerpattern for varying interferer directions for $INR = 70$dB

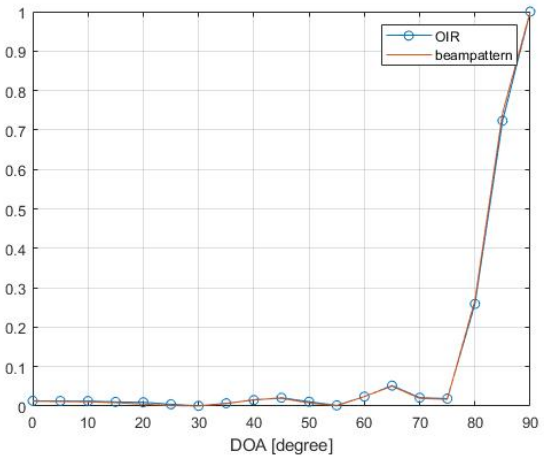

Figure 16: OIR and beampattern - broadside

From Figs. 14 and 15, we can observe that when the INR is high, the power pattern attempts to reduce the directivity noise and exhibits a strong null in its direction. Conversely, in the case of a low INR, the power pattern aims to mitigate all the noise and interference, resulting in a less accurate null.

Exercise 5: Delay-and-Sum Beamformer for Narrowband Signals

The processing of a narrowband signal by a delay-and-sum beamformer (DSB) with $N = 10$ sensors and a sensor spacing of $d = 0.05$ m should be investigated. A single narrowband source signal with a carrier frequency $f_0 = 213$ kHz ($c = 342$ m/s) impinges on the array from different directions $0° \leq \Theta \leq 90°$. The behavior of the beamformer should be investigated by calculating the ratio of the input signal power to the output signal power of the beamformer (output-to-input ratio, OIR). Consider an endfire and broadside orientation and different directions-of-arrival $\Theta = 0°, 5°, \ldots, 90°$.

Compare the calculated OIR with the beampattern of the beamformer. What can be observed?

In Figs. 17 and 16, we can observe that the shape of the OIR in both cases closely resembles the beam pattern. To facilitate comparison, we normalize the OIR to plot both of them on the same scale. Indeed, that makes sense because a narrow-band signal behaves similarly to a monochromatic wave.

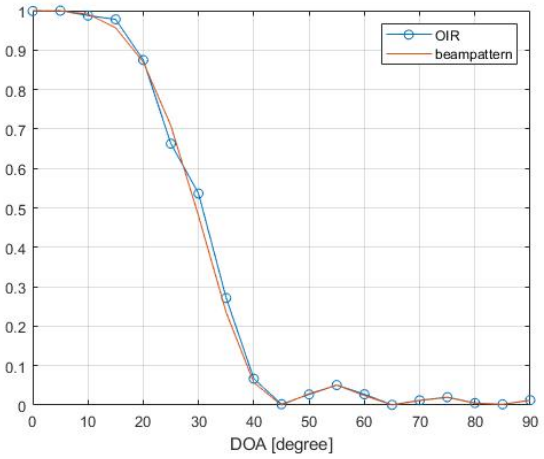

Figure 17: OIR and beampattern - endfire